Molecules and Cells

SMAD4 Controls Cancer Cell Metabolism by Regulating Methylmalonic Aciduria Cobalamin Deficiency (cbl) B Type

Kyoung Song[1,6], Hun Seok Lee[2,6], Lina Jia[3], Chaithanya Chelakkot[4], Nirmal Rajasekaran[5], and Young Kee Shin[2,4,5,*]

[1]College of Pharmacy, Duksung Women's University, Seoul 01366, Korea, [2]Laboratory of Molecular Pathology and Cancer Genomics, Research Institute of Pharmaceutical Sciences and College of Pharmacy, Seoul National University, Seoul 08826, Korea, [3]Department of Pharmacology, Shenyang Pharmaceutical University, Shenyang 110016, China, [4]Bio-MAX Institute, Seoul National University, Seoul 08826, Korea, [5]Department of Molecular Medicine and Biopharmaceutical Sciences, Graduate School of Convergence Science and Technology, Seoul National University, Seoul 08826, Korea, [6]These authors contributed equally to this work.
*Correspondence: ykeeshin@snu.ac.kr
https://doi.org/10.14348/molcells.2022.0067
www.molcells.org

Suppressor of mothers against decapentaplegic homolog (SMAD) 4 is a pluripotent signaling mediator that regulates myriad cellular functions, including cell growth, cell division, angiogenesis, apoptosis, cell invasion, and metastasis, through transforming growth factor β (TGF-β)-dependent and -independent pathways. SMAD4 is a critical modulator in signal transduction and functions primarily as a transcription factor or cofactor. Apart from being a DNA-binding factor, the additional SMAD4 mechanisms in tumor suppression remain elusive. We previously identified methyl malonyl aciduria cobalamin deficiency B type (MMAB) as a critical SMAD4 binding protein using a proto array analysis. This study confirmed the interaction between SMAD4 and MMAB using bimolecular fluorescence complementation (BiFC) assay, proximity ligation assay (PLA), and conventional immunoprecipitation. We found that transient SMAD4 overexpression down-regulates MMAB expression via a proteasome-dependent pathway. SMAD4-MMAB interaction was independent of TGF-β signaling. Finally, we determined the effect of MMAB downregulation on cancer cells. siRNA-mediated knockdown of MMAB affected cancer cell metabolism in HeLa cells by decreasing ATP production and glucose consumption as well as inducing apoptosis. These findings suggest that SMAD4 controls cancer cell metabolism by regulating MMAB.

Keywords: methyl malonyl aciduria cobalamin deficiency B type, mitochondrial energy production, proteasomal pathway, suppressor of mothers against decapentaplegic homolog 4

INTRODUCTION

SMAD4, an SMAD (suppressor of mothers against decapentaplegic homolog) family member, is a central mediator in transforming growth factor β (TGF-β) signaling and transduces extracellular signals to the nucleus (Massague, 1998; Massague and Wotton, 2000). TGF-β signaling activates transmembrane serine-threonine receptor kinases, which phosphorylate SMAD2/3. The phosphorylated SMAD2/3 and their co-mediator SMAD4 translocate to the nucleus, positively or

Received 15 April, 2022; revised 27 April, 2022; accepted 28 April, 2022; published online 3 June, 2022

eISSN: 0219-1032

negatively regulating the target gene transcription (Lee et al., 2021). *SMAD4* is an established tumor suppressor gene that regulates cell cycle arrest, exerts anti-mitogenic and apoptotic effects, and inhibits angiogenesis in early tumor development (Allendorph et al., 2006). It also controls several cellular functions, including cell growth, division, apoptosis, invasion, and metastasis through TGF-β independent pathways (Itatani et al., 2019). It is also the most commonly mutated gene among SMAD family genes. Loss of heterozygosity (LOH), homozygous deletion, intragenic inactivating mutations of the *SMAD4* gene, or complete loss of SMAD4 protein occur in multiple carcinomas causing uncontrolled tumorigenic proliferation either dependent or independent of TGF-β signaling (Bartsch et al., 1999; McCarthy and Chetty, 2018; Miyaki and Kuroki, 2003; Wan et al., 2021; Wilentz et al., 2000). SMAD4 primarily binds DNA by recognizing 8-bps palindromic sequences (GTCTAGAC) known as the SMAD-binding element (Batlle and Massague, 2019; David and Massague, 2018; Zawel et al., 1998). However, SMAD4-mediated events independent of transcriptional regulation are poorly characterized.

MMAB is located at the 12q24 and encodes adenosyltransferase (ATR), which is involved in the intracellular vitamin B_{12} metabolism. *MMAB* mutations are frequently associated with inherited vitamin B_{12} disorders, such as methylmalonic aciduria (Zhang et al., 2006). ATR catalyzes the final step in the conversion of vitamin B_{12} into adenosylcobalamin (AdoCbl), which is a coenzyme essential for methyl malonyl-coenzyme A (CoA) mutase activity (Dobson et al., 2002; Plessl et al., 2017). Methylmalonyl-CoA mutase catalyzes the reversible isomerization of L-methylmalonyl-CoA to succinyl-CoA (Froese and Gravel, 2010). This is an essential catabolic step in energy production, whereby AdoCbl and methylmalonyl-CoA mutase convert carbon skeletons derived from specific amino acids, fatty acids, and cholesterol (lipids) to succinyl-CoA, an intermediate component of the tricarboxylic acid (TCA) cycle. Thus, MMAB interferes with mitochondrial energy production by regulating succinyl-CoA supply to the TCA cycle. Aberrant MMAB expression has been implicated as being linked to cancer. Moderate to intense cytoplasmic MMAB staining in some cancer cells have been previously reported (https://www.proteinatlas.org/ENSG00000139428-MMAB/pathology). However, the mechanism by which MMAB partakes in tumorigenesis is not widely investigated. Here, we identified a novel transcription-independent, tumor suppressive role of SMAD4. We demonstrated that SMAD4 binds MMAB and induces its proteasome-mediated degradation. Furthermore, MMAB downregulation induces apoptosis, which could occur due to compromised mitochondrial energy metabolism.

MATERIALS AND METHODS

Cell culture and transient transfection

The HeLa cervical, A549 lung, and SW480 colon cancer cell lines were purchased from the Korean Cell Line Bank (Korea). They were cultured in an RPMI 1640 medium (Thermo Fisher Scientific, USA) supplemented with 10% fetal bovine serum (Thermo Fisher Scientific) at 37°C in a 5% CO_2 atmosphere. Cells were routinely monitored for mycoplasma contamination and authenticated using short tandem repeat DNA technology. Cells were transfected with 0.5-4 μg of each DNA plasmid using FuGENE® HD (Promega, USA) or with 10-40 nM siRNA using siLentFect (Bio-Rad Laboratories, USA) following the manufacturer's protocol.

Bimolecular fluorescence complementation (BiFC) assay

BiFC constructs using fragments derived from newly engineered fluorescent protein-Venus were kindly provided by Professor Chang-Deng Hu (Department of Medicinal Chemistry and Molecular Pharmacology and Purdue Cancer Center, Purdue University, West Lafayette, IN, USA). cDNAs encoding *SMAD2*, *SMAD2* DNA-binding domains, *SMAD4*, *SMAD4* DNA-binding domains, and *SMAD4* binding candidates identified from ProtoArray, specifically *MMAB* and *MMAB* DNA-binding domains, were amplified using PCR with a human cDNA library. The amplified cDNAs were subcloned into a *pFLAG-CMV* vector to produce BiFC fusion constructs tagged with *VN173* or *VC155*. HeLa cells transfected with BiFC constructs for 24 h were stained with Hoechst 33342 dye (Invitrogen, USA) for nuclei and MitoTracker® Red FM (Invitrogen) for mitochondria. All digital micrograph images were captured using an LSM 700 ZEISS laser scanning confocal microscope (Carl Zeiss, Germany). Prepared cover glass-bottom dishes were observed directly at 20× or 100× magnification (objective lenses) for short-term live cell imaging.

Competition assay

HeLa cells were transiently transfected with *FLAG-VN173-tagged MMAB* (0.5 μg) and *HA-VC155-tagged SMAD4* (0.5 μg) with or without *3 × FLAG-tagged MMAB*. Cells were subjected to BiFC analysis 18 h post-transfection. Detectable fluorescence signals were counted using an LSM 700 ZEISS laser scanning confocal microscope (Carl Zeiss).

Proximity ligation assay (PLA)

PLA experiments were conducted using cultured HeLa cells following the manufacturer's protocol (O-LINK Bioscience, Sweden). HeLa cells were fixed on four-well cell culture slides (SPL Life Sciences, Korea) using 4% paraformaldehyde. After blocking with 5% non-fat milk for 60 min, cells were co-incubated with the primary antibodies, MMAB and SMAD4, at 1:100 dilutions overnight at 4°C. Then, cells were washed twice with TBS-T for five minutes, incubated with PLA probe solutions for 60 min at 37°C, washed twice with TBS-T for five minutes, and incubated with ligase solution for 30 min at 37°C for ligation. After ligation, samples were washed twice with TBS-T for two minutes and incubated with polymerase solution for 100 min at 37°C for amplification. Finally, the samples were washed with SSC buffers (prepared according to the manufacturer's protocol) and ethanol, and subsequently mounted on slides. Slides were imaged using an LSM 700 ZEISS laser scanning confocal microscope. CellLight™ Mitochondria-GFP (Invitrogen) was used to stain HeLa cell mitochondria.

Immunofluorescence

HeLa cells were fixed in 4% paraformaldehyde on an eight-

well cell culture slide (SPL Life Sciences) for double immunofluorescence staining. After fixation, cells were blocked in 5% non-fat milk for 60 min, followed by incubation with primary antibodies against MMAB and SMAD4 at 1:100 dilutions overnight at 4°C. Then, cells were incubated in the secondary antibodies, Alexa Fluor 488-conjugated goat anti-mouse IgG (1:100; Molecular Probes, USA) and Alexa Fluor 546-conjugated goat anti-rabbit IgG (1:100; Molecular Probes), for one hour at room temperature (RT). Finally, samples were washed in phosphate-buffered saline (PBS)/1% Triton X-100 and mounted. Cell nuclei were stained with Hoechst 33342 (Invitrogen). Slides were imaged using an LSM 700 ZEISS laser scanning confocal microscope (Carl Zeiss).

Whole-cell protein extraction and immunoprecipitation (IP)

Cells were collected and washed with PBS. Then, they were extracted in RIPA buffer (150-mM NaCl, 50-mM Tris pH 7.6, 10% Glycerol, 0.1% SDS, and 1% NP40, 0.5% deoxycholic acid) for Western blotting or in IP buffer (25-mM HEPES pH 7.5, 150-mM NaCl, 0.2% NP-40, 10% glycerol, protease and phosphatase inhibitor cocktails) for IP. The supernatant was collected for IP after cell lysis on ice for 20 min and centrifugation at 13,000 × *g* for ten minutes at 4°C. Protein concentrations were determined using a bicinchoninic acid assay (Thermo Fisher Scientific). Proteins were suspended in 5× sodium dodecyl sulfated-polyacrylamide gel electrophoresis (SDS-PAGE) sample buffer for Western blotting. SMAD4 (B8 clone; Santa Cruz Biotechnology, USA) antibody (Biondi et al., 2007) was added to 0.5-mg cell lysate in 800-μl extraction buffer, and this mixture was incubated overnight at 4°C with continuous rotation to allow the formation of immune complexes. To collect immune complexes, 20-μl protein A/G-agarose (50% slurry; Invitrogen) was added to the samples and incubated for two hours. Samples were precipitated via centrifugation at 5,000 × *g* for three minutes, washed thrice with IP wash buffer (25-mM HEPES pH 7.5, 0.2% NP-40, protease and phosphatase inhibitor cocktails), and suspended in 1× SDS-PAGE sample buffer.

Western blotting

Immunoprecipitated samples were subjected to SDS-PAGE (10%-12%) and transferred to polyvinylidene difluoride (PVDF) membranes (Millipore, USA). The membranes were blocked in 5% non-fat milk in TBS-T buffer for 60 min. Primary antibodies against MMAB, HA (3F10 clone; Roche Diagnostics GmbH, Germany), or FLAG (M2 clone; Sigma-Aldrich, USA) were used at 1:1,000 dilutions in 1% non-fat milk in TBS-T buffer for 90 min, followed by washing in TBS-T buffer. Membranes were incubated with an anti-mouse secondary antibody (1:5,000) in TBS-T buffer with 1% non-fat milk for 60 min before washing again in TBS-T buffer for 30 min. Both ACTB (C4 clone; Santa Cruz Biotechnology) and GAPDH (FL335 clone; Santa Cruz Biotechnology) were used as loading controls. The results were visualized with horseradish peroxidase-conjugated secondary antibodies (Thermo Fisher Scientific). Western blot images were developed on photographic film using enhanced chemiluminescence (ECL) reagents (GE Healthcare, USA).

Ubiquitination assay

HeLa cells transiently transfected with *HA-tagged UB* (1 μg) and *FLAG-tagged MMAB* (1 μg), with or without *6MYC-tagged SMAD4* (5 μg), were incubated for 36 h and treated with MG132 (10 μM) or DMSO for six hours before harvest. IP was conducted using an anti-FLAG-M2 antibody (1 μg) with a UB-IP buffer (50-mM Tris pH 7.4, 150-mM NaCl, 0.5% sodium deoxycholate, 1% Triton X-100, protease and phosphatase inhibitor cocktails). Immunoprecipitated samples were washed stringently thrice with UB-wash buffer (50-mM Tris pH 7.4, 1% Triton X-100, protease and phosphatase inhibitor cocktails), boiled at 95°C for ten minutes. The eluted proteins were subjected to Western blotting with anti-FLAG-M2 (Sigma-Aldrich), anti-HA, or anti-MYC antibodies (Santa Cruz Biotechnology).

siRNA sequences

Three siRNAs (*siMMAB-1*, *siMMAB-2*, and *siMMAB-3*) targeting *MMAB* were purchased from TriFECTa® Kit DsiRNA Duplex (Integrated DNA Technologies, USA). The sequences of these siRNAs were GCA GGA AAG ACA GGU AAA GUG AUT G, AGU ACC UUC ACA GGA GAA AGG AGA C, and GGC GGA CAA GAU UUG GAA GUU UAG T, respectively. Optimal siRNA sequence was confirmed by qRT-PCR and western blot. The qRT-PCR primer & probe information are listed in Supplementary Table S1.

Cell proliferation assay

For viable cell counting, 5×10^4 HeLa cells were seeded on a six-well microplate in glucose (conventional RPMI) or pyruvate media, both of which were supplemented with 10% fetal bovine serum and 1% antibiotic for 24 h. The pyruvate medium consisted of RPMI with 10-mM pyruvate (rather than glucose) and 5-mM HEPES (Invitrogen). Then, HeLa cells were transfected with siRNA targeting *MMAB* for 72 h or 120 h, as indicated in the figures. After siRNA transfection, trypan blue dye-excluding live cells were counted using a Countess automated cell counter (Invitrogen). For the kinetic cell proliferation assay, HeLa, A549, and SW480 cells were seeded at 1.25×10^4 cells/well on 96-well microtiter plates (SPL Life Sciences) using a multichannel pipette and cultured in a complete medium (including 10% fetal bovine serum) for 24 h. Then, 10-nM non-targeting or *MMAB*-targeting siRNAs were transfected into each well, and cell plates were incubated in an IncuCyte™ ZOOM (Essen BioScience, USA) and scanned hourly for 72 h or 120 h.

ATP production and glucose consumption

Cellular ATP levels were determined using a CellTiter-Glo® luminescent cell viability assay kit (Promega). Briefly, 4×10^3 HeLa cells were seeded on an opaque-walled 96-well microplate and transfected for 120 h at 37°C with non-targeting or *MMAB*-targeting siRNA. After equilibrating microplates via incubation for 30 min at RT, 100-μl CellTiter-Glo® reagent was added to 100-μl medium containing cells, and the plate was rotated for two minutes on an orbital shaker to induce cell lysis. Finally, plates were incubated for ten minutes at RT to stabilize the luminescent signal. The cells were imaged and recorded using a GENios reader (Tecan, Switzerland).

A glucose assay kit (Sigma-Aldrich) was used to measure glucose consumption. Briefly, 1×10^5 *MMAB* siRNA-transfected HeLa cells in a 6-well plate were incubated for 60 h at 37°C. Then, the medium was mixed with glucose assay reagent, transferred into 96-well microplates, and incubated for 30 min at 37°C. Microplates were measured at 540-nm using a GENios reader (Tecan).

Kinetic caspase-3/7 apoptosis assay

Briefly, *siMMAB*-transfected cell apoptosis was measured using kinetic caspase-3/7 apoptosis reagent (Essen BioScience) following the manufacturer's protocol. HeLa cells were transfected with non-targeting or *MMAB*-targeting siRNAs in the presence of 5-μM caspase 3/7 reagent. Phase contrast and green fluorescence images were captured hourly using an IncuCyte™ ZOOM (20× objective) (Essen BioScience).

Seahorse energy phenotype assay

The metabolic phenotype of *siMMAB*-transfected HeLa cells was measured using a seahorse energy phenotype assay kit (Agilent Technologies, USA). Briefly, 1×10^4 HeLa cells were seeded into 96-well cell culture microplates, followed by siRNA transfection the next day. The seahorse assay was conducted 48 h after siRNA transfection. The sensor cartridge was hydrated in sterile water overnight in a non-CO_2 37°C incubator for the seahorse assay. After hydration, the sensors were calibrated using a calibrant solution for 45 min in a non-CO_2 37°C incubator. On the day of the assay, cell culture plates were washed twice with assay medium (Seahorse XF medium supplemented with 2-mM glutamine, 1-mM pyruvate, and 10-mM glucose), 180-μl assay medium was added to each well and incubated in a non-CO_2 37°C incubator for 30 min. A stressor mixture of oligomycin (1-μM), FCCP (1-μM), and Hoechst 33342 for nuclear staining was added to port A of the cartridge, and an energy phenotype test was conducted following the manufacturer's protocol. The assay was normalized via nuclear staining of cells, and cell counts derived from images were captured using Cytation 1 cell imaging system (BioTek Instruments, USA). The results were analyzed using a wave software (Agilent Technologies).

Statistical analyses

IBM SPSS Statistics software (ver. 21; IBM, USA) was used for statistical analyses. A Mann–Whitney test was used to compare cell viability, ATP production, glucose consumption, reactive oxygen species generation, apoptosis, and senescence data between the two groups. Data were expressed as the mean ± SD or standard error of the mean, calculated from three or more independent experiments. Additional methods are given in Supplementary Materials and Methods.

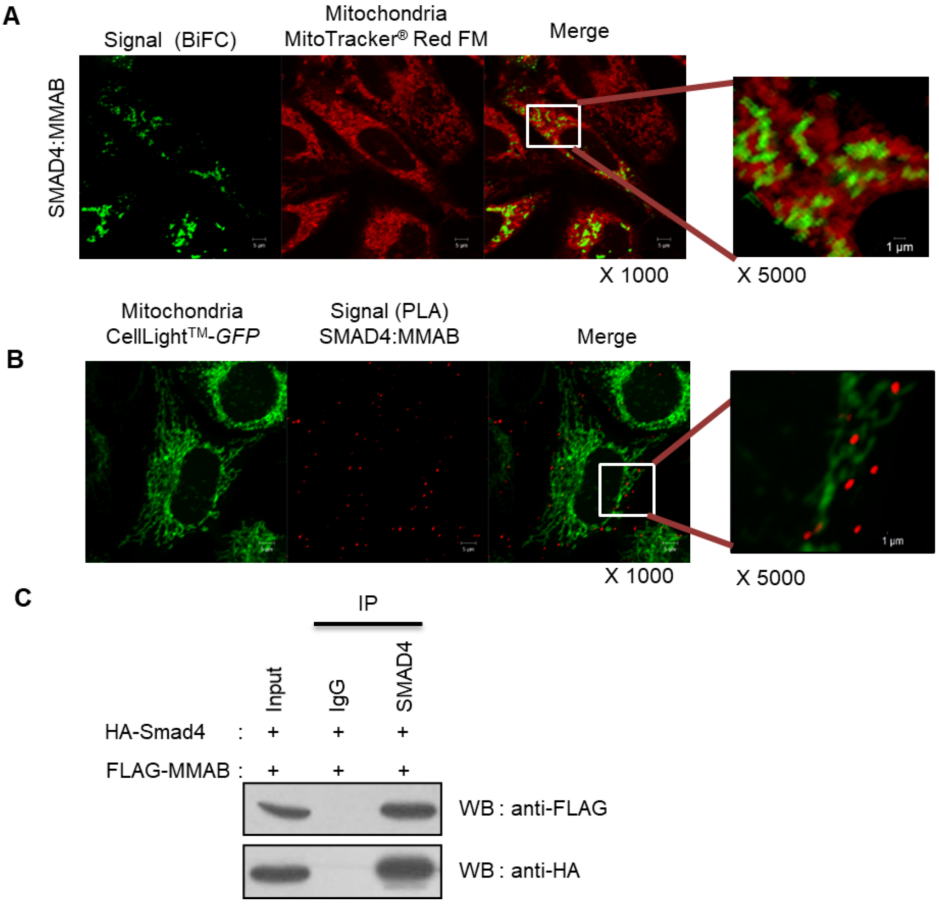

Fig. 1. Cytosolic SMAD4-MMAB binding. (A) Cytosolic SMAD4-MMAB binding was evaluated using a BiFC assay. Co-expression of *SMAD4* and *MMAB* produced a fluorescent signal, which was indicative of direct interaction. Scale bars = 5 μm. Magnified images revealed that the interactions did not occur in the mitochondria. Scale bar = 1 μm. (B) SMAD4-MMAB interaction was evaluated by *in situ* PLA. The SMAD4-MMAB interaction is indicated by red signals. HeLa cell mitochondria were stained with CellLight™-Mitochondria-GFP (green). Magnified images demonstrated that the interaction did not occur in mitochondria. Scale bars = 5 μm for all images. Scale bar for magnified image is 1 μm. (C) Co-immunoprecipitation (IP) analysis was suggestive of a physical interaction between SMAD4 and MMAB.

RESULTS

SMAD4 specifically binds MMAB in the cytosol

We conducted a eukaryotic-expressed human protein array (ProtoArray) with purified SMAD4, identifying the mitochondrial protein, MMAB, as a novel SMAD4 binding protein (Rajasekaran et al., 2021). The SMAD4 and MMAB interaction was assessed using a BiFC assay, allowing the detection of the subcellular localization of the SMAD4-MMAB complex in live cells. We observed the cytosolic interaction between SMAD4 and MMAB; however, the BiFC signals from the SMAD4-MMAB complex did not overlap with mitochondria, as confirmed by MitoTracker® Red FM staining (Fig. 1A). The specificity of the SMAD4 and MMAB interaction was checked in the presence of the *3×FLAG*-MMAB construct, functioning as a competitor, potentially inhibiting the interaction between *VC*-SMAD4 and *VN*-MMAB. We found that *3×FLAG*-MMAB dose-dependently decreased the BiFC signal between *VC*-SMAD4 and *VN*-MMAB (Supplementary Fig. S1), suggesting that a specific protein-protein interaction mediates the fluorescence complementation. In the competition assay, levels of each exogenously expressed protein were stably maintained, demonstrating that the decreased BiFC signal did not occur due to altered SMAD4 or MMAB levels, but due to the SMAD4 and MMAB interaction with the competitor. The interaction between endogenous SMAD4 and MMAB was further verified in HeLa cells using an *in situ* PLA after labeling mitochondria with CellLight™ Mitochondria-GFP (Fig. 1B). Individual SMAD4-MMAB complexes were visualized as red spots in the cytosol, and the complexes did not colocalize to mitochondria. Conventional IP of HeLa cell lysates verified the interaction between SMAD4 and MMAB. *FLAG*-tagged MMAB co-immunoprecipitated with *HA*-tagged SMAD4, which was consistent with the proposed SMAD4-MMAB interaction (Fig. 1C). These results confirmed the specific interaction between SMAD4 and MMAB in the cytosol.

SMAD4-linker domain binding to the MMAB catalytic domain

To identify the protein binding domains responsible for the SMAD4-MMAB interaction, we designed *SMAD4* and *MMAB* constructs encoding only discrete functional domains. *HA-VC155*-Full *SMAD4* was co-expressed in HeLa cells expressing either the MMAB signal peptide (*FLAG-VN173-MMAB* signal peptide) or the MMAB catalytic domain (*FLAG-VN173-MMAB* catalytic domain). The BiFC fluorescence signal suggested an interaction between full-length SMAD4 and the MMAB catalytic domain (Fig. 2A). In contrast, when full-length *MMAB* was co-expressed with each of the five SMAD4 truncated constructs, interaction occurred between MMAB and the SMAD4-linker domain, flanked by the MH1 and MH2 domains (Fig. 2B). Because linker domains vary in size depending on the SMAD family member, unlike the conserved MH1 and MH2 domains, we determined whether other SMAD family members interact with MMAB. Interestingly, MMAB did not bind to other SMAD family members (Supplementary Fig. S2).

SMAD4 is a major component of TGF-β signaling. Hence, we investigated whether the SMAD4-MMAB interaction

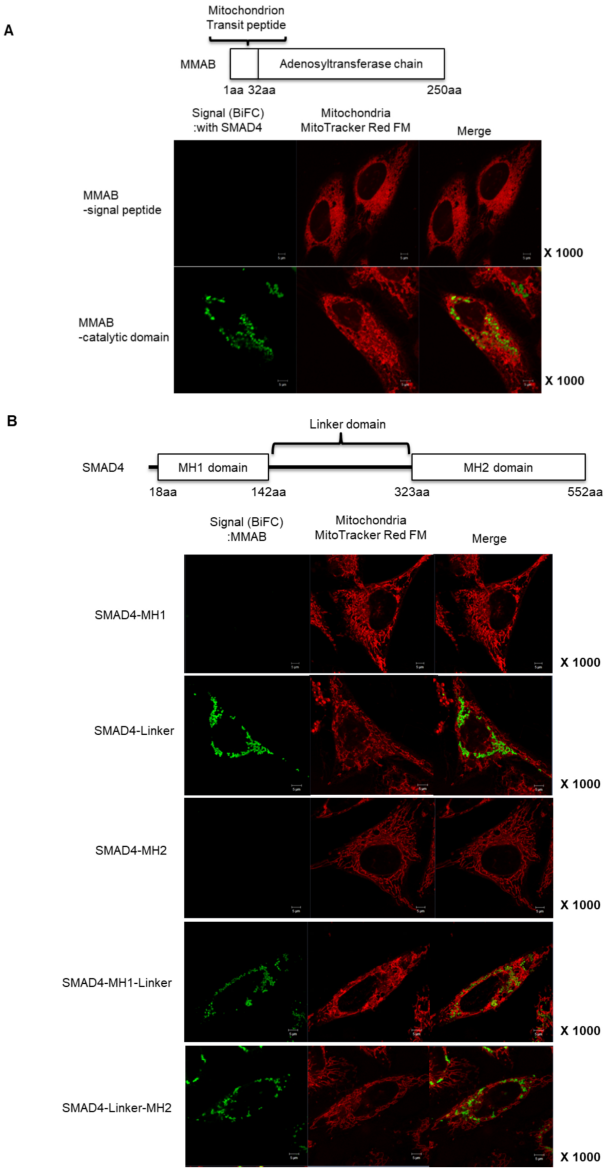

Fig. 2. Interaction of SMAD4-Linker domain with MMAB catalytic domain. (A) BiFC analysis with either *SMAD4:truncated MMAB mutants* or (B) *MMAB:truncated SMAD4mutants*. Interaction between SMAD4 and MMAB is indicated by green fluorescence and mitochondria are labeled with a red signal. Scale bars = 5 μm.

was TGF-β-dependent or not. HeLa cells transfected with BiFC constructs (*VC-SMAD4* and *VN-MMAB*) were treated with TGF-β for zero, one, or 24 h. The intensity of the signal generated by the SMAD4-MMAB interaction was not affected by TGF-β treatment. This shows that the interaction is TGF-β-independent (Fig. 3).

SMAD4 decrease MMAB Levels via a proteasome-dependent pathway

Subsequently, we investigated the signaling downstream of the SMAD4-MMAB interaction. SMAD4 expression de-

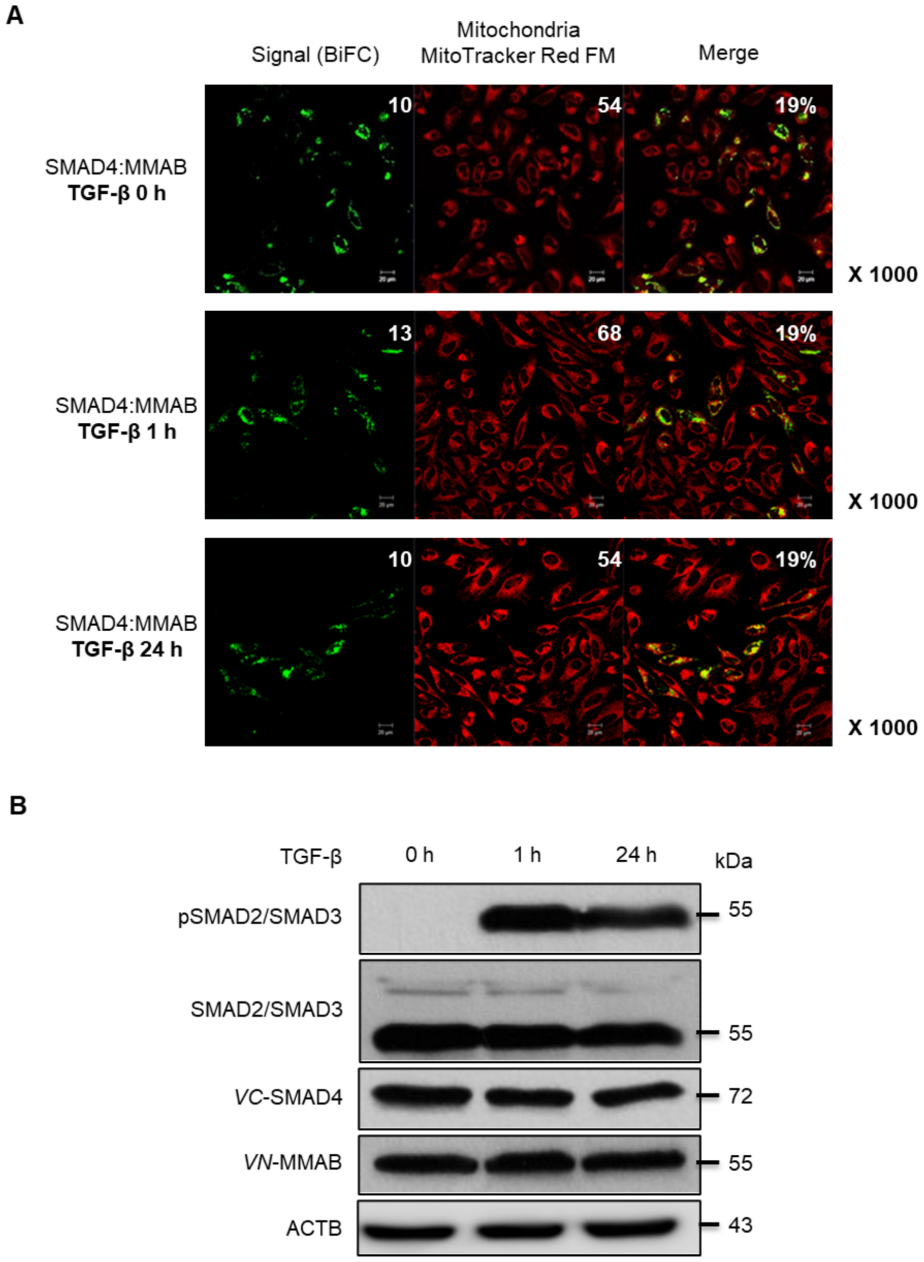

Fig. 3. TGF-β-signaling independent interaction of SMAD4 and MMAB. (A) Changes of the interaction between SMAD4 and MMAB with TGF-β treatment for 1 h or 24 h. Images were acquired 24 h after transfection. Scale bars = 20 μm. The green signal is indicative of SMAD4-MMAB interaction and red signal is indicative of mitochondria. (B) Western image showing the expression changes of MMAB and SMAD4 after TGF-β treatment.

creased both exogenous and endogenous *MMAB* expression (Figs. 4A and 4B). Additionally, the induction of exogenous *SMAD4* expression in the SNU601 cell line, which lacks endogenous SMAD4, decreased the MMAB expression (Fig. 4C). Furthermore, we investigated the mechanism of SMAD4-mediated MMAB downregulation. To determine whether SMAD4-mediated MMAB downregulation occured due to proteasomal degradation, HeLa cells transfected with 6*MYC-SMAD4* were treated for six hours with the 26S proteasome inhibitor MG132 (10 μM). SMAD4-mediated MMAB downregulation was abrogated by treatment with MG132, suggesting that SMAD4 decreases MMAB levels via a proteasome-dependent pathway (Fig. 4D). We also demonstrated that in the presence of exogenous *HA-UB*, SMAD4-induced proteasomal MMAB degradation was blocked by the MG132 treatment (Fig. 4E). Our results indicate that SMAD4 induces MMAB degradation via a proteasome-dependent pathway.

MMAB downregulation induces cell death

To determine the effects of MMAB downregulation, siRNA targeting *MMAB* was employed. Efficient *MMAB* siRNA (*siMMAB*) was screened and selected from three candidate sequences (Supplementary Fig. S3), of which *siMMAB-1* demonstrated the most efficient gene silencing. Cancer cells (HeLa, A549, and SW480) were transiently transfected for five days with 10-nM *siMMAB-1*. *MMAB* knockdown significantly decreased HeLa cell viability (Supplementary Fig. S4). To elucidate the cytotoxic effects of MMAB depletion,

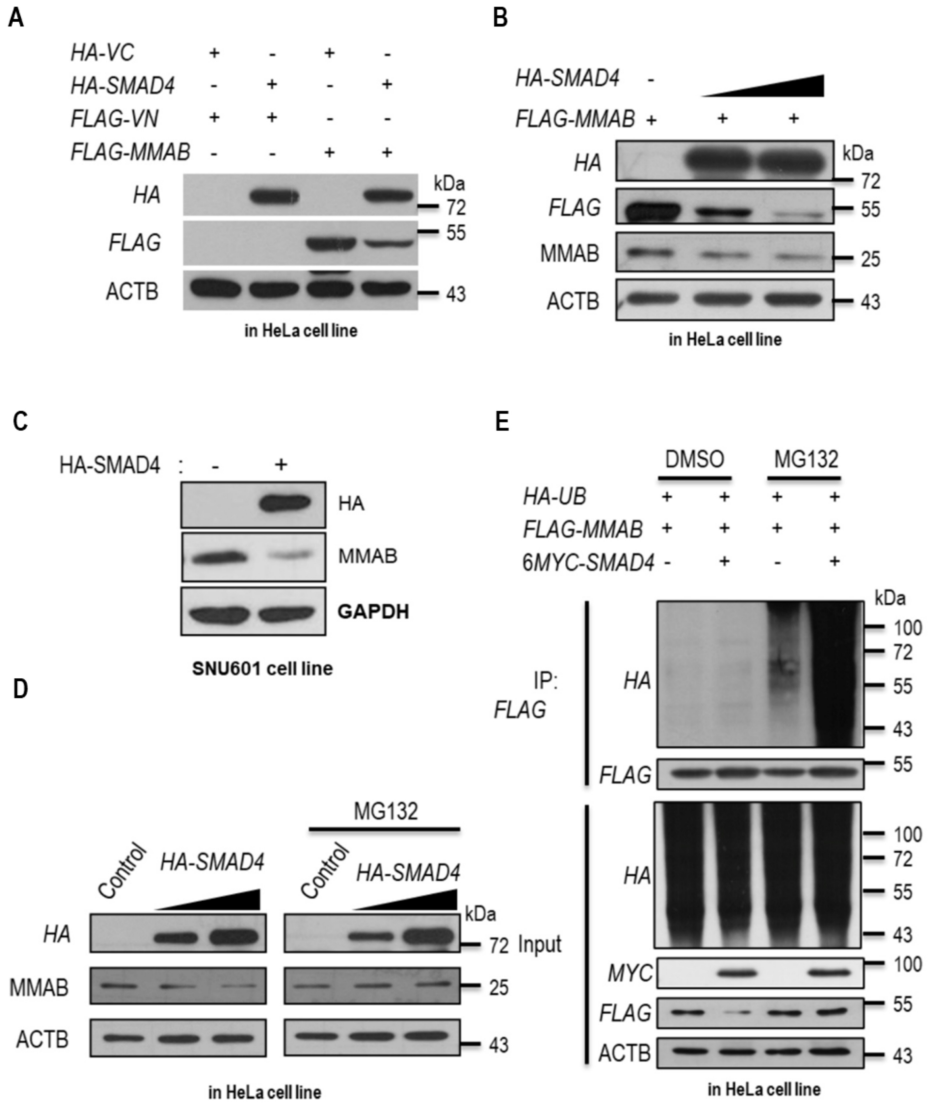

Fig. 4. Protesomal degradation and downregulation of MMAB by SMAD4. (A) SMAD4 decreases exogenous MMAB protein levels. HeLa cells were co-transfected with *HA-SMAD4*, *FLAG-MMAB*, and/or empty vector. (B) Ectopic expression of SMAD4 decreases endogenous MMAB. HeLa cells were transfected with *FLAG-MMAB* and different doses of the *HA-SMAD4* expression vector for 48 h. Total cell extracts were analyzed by immunoblotting using the indicated antibodies. (C) Restoration of SMAD4 protein decreases endogenous MMAB protein levels. *HA-SMAD4* was transfected into SNU601 cells, a SMAD4-deficient cell line. (D) Degradation of MMAB mediated by SMAD4 expression is restored by the 26S proteasome inhibitor MG132. (E) Ubiquitination of MMAB mediated by SMAD4. HeLa cells were transfected with *FLAG-MMAB* and *HA-ubiquitin* together with or without *6MYC-SMAD4* as indicated. Cell lysates were subjected to immunoprecipitation (IP) with a FLAG antibody and then reprecipitated by protein G beads prior to immunoblotting.

we imaged *siMMAB*-transfected HeLa cells hourly for 72 h or 120 h using real-time live cell imaging (Supplementary Movies A and B). Cell proliferation was kinetically determined while monitoring the morphological changes. In contrast to non-targeting control siRNA transfection, *siMMAB* transfection significantly increased cell death after 48 h (Fig. 5A). Since *MMAB* knockdown increased cell death, we investigated whether *MMAB* knockdown induced apoptosis. Caspase-3 activation is considered a suitable marker for cells undergoing canonical apoptosis. We measured HeLa cell viability after MMAB depletion using a ZOOM™ imaging system with an Essen CellPlayer™ Kinetic Caspase-3/7 apoptosis reagent, a non-fluorescent substrate that emits green fluorescence after cleavage by activated caspase-3/7 (Cen et al., 2008). Caspase-3/7 activation was detected in cells transfected with *siMMAB* (Fig. 5B, Supplementary Movie C). Treatment with the caspase/apoptosis inhibitor z-VAD-FMK significantly decreased *siMMAB*-induced cell death; however, cell death was incompletely restored to the level of non-targeting siRNA-transfected cells (Fig. 5C, Supplementary Movies D and E). Hence, it can be interpreted from the above results that MMAB downregulation induces cell death via apoptosis.

MMAB depletion affects mitochondrial energy metabolism

The role of MMAB in cancer is incompletely understood. MMAB is involved in converting L-methylmalonyl-CoA to succinyl-CoA, a TCA cycle intermediate. We postulated that the SMAD4-mediated downregulation of MMAB inhibits the production of succinyl-CoA, thereby inhibiting the TCA cycle. Thus, we investigated whether MMAB depletion decreased ATP production and compromised energy metabolism. MMAB depletion significantly decreased ATP production and glucose consumption in HeLa cells (Figs. 6A and 6B). Since glucose is a component of normal cell culture medium, ATP could be produced by both glycolysis and the TCA cycle under these conditions. Thus, to determine whether MMAB downregulation affected the TCA cycle, we examined the effect of *siMMAB* on cell viability in culture media supplemented with pyruvate rather than glucose. Cell death of *siMMAB*-trans-

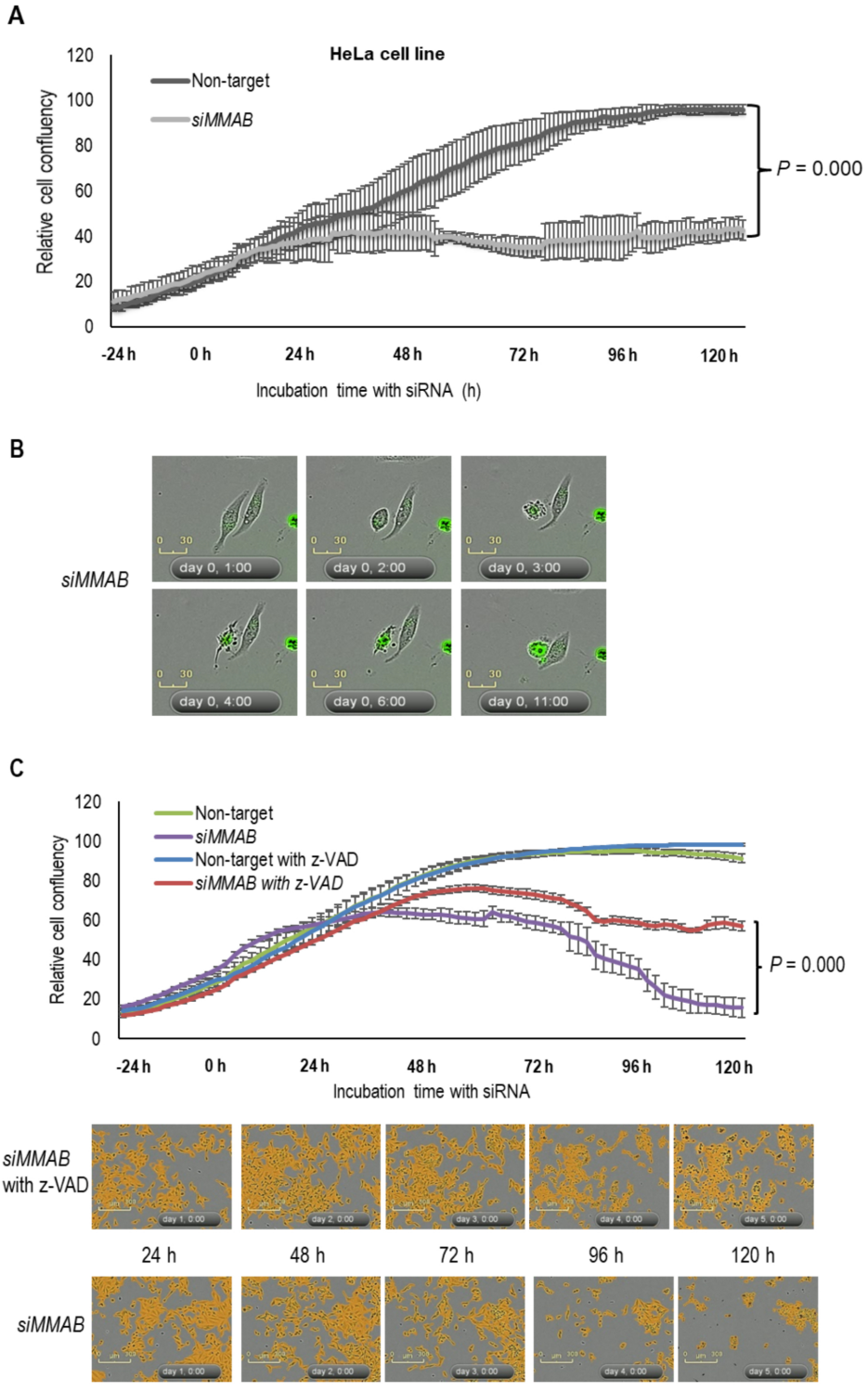

Fig. 5. Apoptosis induced by MMAB knockdown. (A) *siMMAB* decreases cancer cell proliferation. HeLa cells were transfected with 10 nM non-targeting or *MMAB*-targeting siRNAs and relative cell confluency was monitored for 120 h. $P < 0.05$ was considered statistically significant. (B) Depletion of MMAB induces caspase 3/7-mediated apoptosis. HeLa cells were transfected with 10 nM non-targeting or *MMAB*-targeting siRNAs. The number of caspase-3/7-positive cells was monitored in the same areas of the wells for 72 h using real-time live cell imaging. Scale bar = 30 μm. (C) Top panels: Apoptosis of HeLa cells transfected with 10 nM *siMMAB* is inhibited by co-treatment with the caspase/apoptosis inhibitor z-VAD-FMK. Bottom panels: Cell growth and morphology were monitored in the same areas of the wells for 120 h using real-time live cell imaging. Classical morphological changes were observed using phase contrast images (4×, objective lens). $P < 0.05$ was considered statistically significant. Yellow masks represent cell confluency. Scale bar = 300 μm.

fected HeLa cells cultured in glucose-free medium supplemented with pyruvate was more significant than that in glucose-containing media. These results suggest that MMAB depletion potentially decreases cell viability by suppressing the TCA cycle in mitochondria (Fig. 6C, Supplementary Movies F and G). MMAB suppression could compromise the TCA cycle and inhibit glycolysis. A seahorse energy phenotype assay was conducted to further assess the effects of MMAB knockdown on energy metabolism. Consistent with our earlier findings, *MMAB* knockdown decreased the oxygen consumption rate (OCR) and extracellular acidification rate (ECAR) in HeLa cells (Figs. 6D and 6E). These findings suggest that *MMAB* knock-

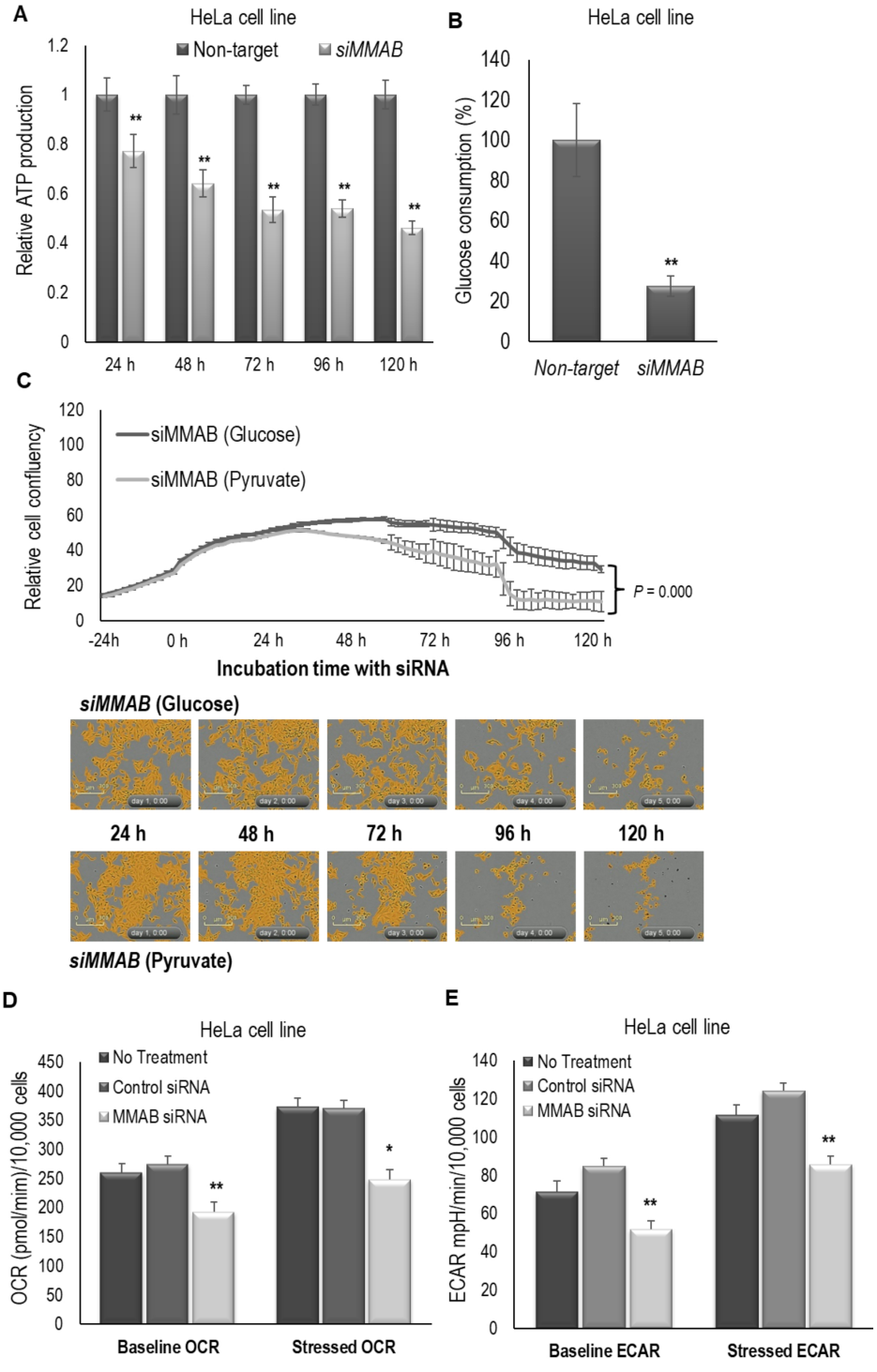

Fig. 6. Mitochondrial energy metabolism changes from MMAB knockdown. (A) HeLa cells transfected with 10 nM *MMAB* siRNA displayed significant decreases in intracellular ATP levels for 120 h relative to control cells. $**P < 0.01$. (B) HeLa cells transfected with 10 nM *MMAB* siRNA for 40 h consumed glucose at a much lower rate than control cells. $**P < 0.01$. (C) *siMMAB* increases cell death by inhibiting mitochondrial ATP synthesis. Top panels: HeLa cells were transfected with 10 nM siRNA targeting *MMAB* in RPMI medium (glucose) or RPMI medium (pyruvate). Bottom panels: Cell growth and morphology were monitored in the same areas of the wells for 120 h using real-time live cell imaging. Apoptotic morphological changes were observed using phase contrast images (4× objective lens). $P < 0.05$ was considered statistically significant. Yellow masks represent cell confluency. Scale bars = 300 μm. (D) siRNA-mediated *MMAB* knockdown significantly decreased baseline and stressed OCR in HeLa cells relative to control and non-treated cells. $*P < 0.05$, $**P < 0.01$. (E) siRNA-mediated *MMAB* knockdown significantly decreased ECAR under both baseline and stressed conditions in HeLa cells compared with control and non-treated cells. $**P < 0.01$.

down increases cancer cell death by indirectly inhibiting the TCA cycle, as implicated by decreased OCR and ECAR.

DISCUSSION

The role of SMAD4 as a tumor suppressor has been extensively studied (Schutte, 1999). SMAD4 inactivation is mediated by LOH, loss-of-function mutations, downregulation via promoter hypermethylation, and ubiquitin proteosome-mediated degradation. The deregulation of the nuclear-cytoplasm SMAD4 shuttle is implicated in the development and progression of different cancers, including pancreatic, gastrointestinal, and colorectal cancers (Bardeesy et al., 2006; Blackford et al., 2009; Papageorgis et al., 2011; Yan et al., 2016). The anti-tumorigenic mechanisms of SMAD4 are mediated by its DNA-binding functions, where SMAD4 acts as a transcription

factor or cofactor (Johnson et al., 1999; McCarthy and Chetty, 2018). Here we describe a novel mechanism underlying the anti-tumor effects of SMAD4.

Our previous protein array study identified MMAB as a novel SMAD4 binding partner (Rajasekaran et al., 2021). Although the inhibitory effects of SMAD4 on cancer progression are well-known, the regulatory mechanisms independent of its transcriptional function are poorly understood. Additionally, studies on how MMAB is involved in cancer cells' metabolism remain infant (Chan et al., 2015; Sorin et al., 2021; Gomes et al., 2022). Here, to the best of our knowledge, we identified for the first time that SMAD4 suppresses tumorigenesis by decreasing MMAB and disrupting cancer cell energy metabolism by inhibiting the TCA cycle.

Firstly, we demonstrated that cytosolic SMAD4-MMAB binding is TGF-β-independent. The SMAD4-linker domain specifically interacts with the MMAB catalytic domain. SMAD4-MMAB binding decreased MMAB protein levels by inducing proteasomal MMAB degradation. SMAD4-mediated decrease in MMAB levels was mimicked using *siMMAB*. siRNA-mediated *MMAB* downregulation significantly decreased HeLa cell viability, suggesting cancer-promoting effects of MMAB (Fig. 5A).

MMAB is involved in AdoCbl synthesis, an activated form of vitamin B_{12} that is a required enzymatic cofactor of methylmalonyl-CoA mutase, converting methylmalonyl-CoA to succinyl-CoA (Dobson et al., 2002). The loss of enzyme activity or cofactors for this reaction as well as consequent methylmalonic acid accumulation, can disrupt normal glucose metabolism (Rosenberg et al., 1968a; 1968b). Anaplerotic deficiencies of the TCA cycle are frequently observed in patients with methylmalonyl aciduria, a disease characterized by methylmalonic acid accumulation (Anzmann et al., 2019). Genome-wide association studies have identified that single-nucleotide polymorphisms in the *MMAB* gene are strongly associated with breast cancer (Haiman et al., 2013). However, the underlying regulatory mechanisms for the role of MMAB in cancer progression are largely unexplored.

Here, based on the role of MMAB in providing substrates for the TCA cycle, we postulated that MMAB could be related to mitochondrial energy metabolism, promoting the TCA cycle. Through the downregulation of MMAB by interaction with SMAD4, the suppression of methylmalonyl-CoA mutase expression decreased the succinyl-CoA synthesis. Thus, the supply of succinyl-CoA ultimately becomes insufficient to sustain the mitochondrial energy production via the TCA cycle. Therefore, the decreased succinyl-CoA production interferes with the TCA cycle function. We observed that cell viability significantly decreased 72 h after *MMAB* knockdown. Thus, cell death resulting from MMAB depletion could be due to deficient ATP production and glucose consumption (Figs. 6A and 6B). Seahorse assay also exhibited a reduction in OCR and ECAR in cells with MMAB downregulation (Figs. 6D and 6E). The observed reduced OCR occurred likely due to a reduction in succinyl co-A supply to the TCA cycle, which is a major substrate entry point in the TCA cycle. Also, succinyl co-A conversion to succinate is associated with the generation of energy-rich phosphates (Anderson et al., 2018; Inigo et al., 2021; Rush et al., 2014). This energy-providing pathway of succinyl co-A conversion is extremely important when energy production via oxidative phosphorylation is inhibited, explaining the reduced ATP production (Phillips et al., 2009). Interestingly, TCA cycle inhibition by MMAB downregulation did not improve glycolysis or glucose consumption through a compensative pathway, but rather reduced glucose consumption. Earlier studies have identified the relationship between vitamin B_{12} deficiency in the glycolytic and citric acid cycle. Though vitamin B_{12} deficiency is directly associated with intermediates of the TCA cycle, a general reduction in energy utilization has been documented, which might in turn result in feedback inhibition of glucose consumption (Depient et al., 2006; Fehling et al., 1979). The accumulation of TCA cycle intermediates is also associated with glycolysis inhibition. However, the direct effect of MMAB on glycolytic enzymes is not understood, and further experiments are essential to understand the association.

The depletion of cellular ATP is a crucial event that mediates cell death. Notably, previous studies have demonstrated that apoptosis is an ATP-dependent process and that decreased ATP levels promote cell death (Ferrari et al., 1998; Tsujimoto, 1997; Zamaraeva et al., 2005). Decreased ATP levels could occur due to the direct role of succinyl-CoA in ATP production via the TCA cycle, or an indirect effect due to TCA cycle inhibition (Williamson and Cooper, 1980). Therefore, proteasomal MMAB degradation regulated by the SMAD4-MMAB interaction primarily inhibits mitochondrial ATP synthesis due to alterations in the levels of TCA cycle intermediates, consequently activating caspase 3-mediated apoptosis. Further in-depth studies are essential to understand the input of other TCA cycle intermediates and anaplerotic substrates in inhibiting ATP production.

In contrast to the conventional belief that cancer cells bypass the TCA cycle and rely primarily on glycolysis (Pavlova and Thompson, 2016), recent studies have demonstrated that cancer cells with defective tumor suppressor mechanisms and oncogenic mutations depend on the TCA cycle for sufficient ATP production and survival (Anderson et al., 2018). Exploiting these unique metabolic dependencies opens a new horizon for targeted cancer therapies (Lee and Kim, 2016; Pathania et al., 2009). Several components of the TCA cycle, including α-ketoglutarate dehydrogenase (KGDHC), isocitrate dehydrogenase (IDH), and pyruvate dehydrogenase (PDH), are emerging as compelling anti-cancer therapeutic targets (Allen et al., 2016; Dang et al., 2009; Zachar et al., 2011). Recently, CPI-613 (Devimistat), a molecule that simultaneously inhibits KGDHC and PDH, is being investigated in clinical trials as a stand-alone therapy or along with chemotherapy (Lycan et al., 2016; Pardee et al., 2014). Small molecule inhibitors of IDH; AG-221 and AG-881, are also involved in clinical development (Yen et al., 2017). However, the dependency of normal cells on the TCA cycle for ATP production is likely to induce off-target cytotoxic effects, posing a significant barrier to this approach. Recent studies also demonstrated that cancer cells use the TCA cycle differently than normal cells, thereby increasing their sensitivity to TCA cycle inhibitors (Grassian et al., 2014; Kishton and Rathmell, 2016; Yuneva et al., 2012). In this study, we identified MMAB as a novel SMAD4 binding partner, and identified

that SMAD4-MMAB interaction decreases MMAB protein levels in cancer cells, primarily inducing cell death via TCA cycle inhibition. Although the role of MMAB in cancer has not been widely investigated, public databases, such as the human protein atlas, intriguingly revealed increased MMAB protein levels in various cancerous tissue samples.

This prompted us to propose the previously untested hypothesis that normal cells could transform into cancer cells *in vivo*. In normal cells, SMAD4 maintains stable MMAB levels, which could be an ideal strategy to maintain the characteristics of normal cells, not to be biased to apoptosis or cancerous pathway. If genetic alterations, including gain-of-function *MMAB* mutations or *SMAD4* deletion occur, this equilibrium would be disrupted, and consequent MMAB overexpression could promote aberrant cancer cell proliferation due to increased energy production. Thus, targeting MMAB could be a promising strategy to indirectly target the TCA cycle, thereby inducing cancer cell apoptosis. This novel finding provides broadly applicable mechanistic insights into tumorigenesis, facilitating the identification of novel therapeutic targets.

Note: Supplementary information is available on the Molecules and Cells website (www.molcells.org).

ACKNOWLEDGMENTS

Authors would like to extend their thanks to Professor Chang-Deng Hu (Department of Medicinal Chemistry and Molecular Pharmacology and Purdue Cancer Center, Purdue University, West Lafayette, IN) for kindly gifting them the BiFC constructs using fragments derived from newly engineered fluorescent protein-Venus.

AUTHOR CONTRIBUTIONS

K.S., H.S.L., and Y.K.S. conceived and conceptualized the manuscript. Y.K.S. supervised and administered the project, and acquired the fund. K.S., H.S.L., C.C., N.R., and L.J. performed the experiments and acquired the data. K.S., H.S.L., and C.C. wrote the original draft. K.S., C.C., and Y.K.S. wrote, reviewed, and edited the final manuscript. All authors have read and agreed to the published version of this manuscript.

CONFLICT OF INTEREST

The authors have no potential conflicts of interest to disclose.

ORCID

Kyoung Song https://orcid.org/0000-0003-3123-5745
Hun Seok Lee https://orcid.org/0000-0001-6150-5510
Lina Jia https://orcid.org/0000-0002-2845-7286
Chaithanya Chelakkot https://orcid.org/0000-0002-4548-5510
Nirmal Rajasekaran https://orcid.org/0000-0001-7400-4387
Young Kee Shin https://orcid.org/0000-0003-0896-718X

REFERENCES

Allen, E.L., Ulanet, D.B., Pirman, D., Mahoney, C.E., Coco, J., Si, Y., Chen, Y., Huang, L., Ren, J., Choe, S., et al. (2016). Differential aspartate usage identifies a subset of cancer cells particularly dependent on OGDH. Cell Rep. *17,* 876-890.

Allendorph, G.P., Vale, W.W., and Choe, S. (2006). Structure of the ternary signaling complex of a TGF-beta superfamily member. Proc. Natl. Acad. Sci. U. S. A. *103,* 7643-7648.

Anderson, N.M., Mucka, P., Kern, J.G., and Feng, H. (2018). The emerging role and targetability of the TCA cycle in cancer metabolism. Protein Cell *9,* 216-237.

Anzmann, A.F., Pinto, S., Busa, V., Carlson, J., McRitchie, S., Sumner, S., Pandey, A., and Vernon, H.J. (2019). Multi-omics studies in cellular models of methylmalonic acidemia and propionic acidemia reveal dysregulation of serine metabolism. Biochim. Biophys. Acta Mol. Basis Dis. *1865,* 165538.

Bardeesy, N., Cheng, K.H., Berger, J.H., Chu, G.C., Pahler, J., Olson, P., Hezel, A.F., Horner, J., Lauwers, G.Y., Hanahan, D., et al. (2006). Smad4 is dispensable for normal pancreas development yet critical in progression and tumor biology of pancreas cancer. Genes Dev. *20,* 3130-3146.

Bartsch, D., Hahn, S.A., Danichevski, K.D., Ramaswamy, A., Bastian, D., Galehdari, H., Barth, P., Schmiegel, W., Simon, B., and Rothmund, M. (1999). Mutations of the DPC4/Smad4 gene in neuroendocrine pancreatic tumors. Oncogene *18,* 2367-2371.

Batlle, E. and Massague, J. (2019). Transforming growth factor-beta signaling in immunity and cancer. Immunity *50,* 924-940.

Biondi, C.A., Das, D., Howell, M., Islam, A., Bikoff, E.K., Hill, C.S., and Robertson, E.J. (2007). Mice develop normally in the absence of Smad4 nucleocytoplasmic shuttling. Biochem. J. *404,* 235-245.

Blackford, A., Serrano, O.K., Wolfgang, C.L., Parmigiani, G., Jones, S., Zhang, X., Parsons, D.W., Lin, J.C., Leary, R.J., Eshleman, J.R., et al. (2009). SMAD4 gene mutations are associated with poor prognosis in pancreatic cancer. Clin. Cancer Res. *15,* 4674-4679.

Cen, H., Mao, F., Aronchik, I., Fuentes, R.J., and Firestone, G.L. (2008). DEVD-NucView488: a novel class of enzyme substrates for real-time detection of caspase-3 activity in live cells. FASEB J. *22,* 2243-2252.

Chan, R., Mascarenhas, L., Boles, R.G., Kerkar, N., Genyk, Y., and Venkatramani, R. (2015). Hepatoblastoma in a patient with methylmalonic aciduria. Am. J. Med. Genet. A *167A,* 635-638.

Dang, L., White, D.W., Gross, S., Bennett, B.D., Bittinger, M.A., Driggers, E.M., Fantin, V.R., Jang, H.G., Jin, S., Keenan, M.C., et al. (2009). Cancer-associated IDH1 mutations produce 2-hydroxyglutarate. Nature *462,* 739-744.

David, C.J. and Massague, J. (2018). Contextual determinants of TGFbeta action in development, immunity and cancer. Nat. Rev. Mol. Cell Biol. *19,* 419-435.

Depeint, F., Bruce, W.R., Shangari, N., Mehta, R., and O'Brien, P.J. (2006). Mitochondrial function and toxicity: role of B vitamins on the one-carbon transfer pathways. Chem. Biol. Interact. *163,* 113-132.

Dobson, C.M., Wai, T., Leclerc, D., Kadir, H., Narang, M., Lerner-Ellis, J.P., Hudson, T.J., Rosenblatt, D.S., and Gravel, R.A. (2002). Identification of the gene responsible for the cblB complementation group of vitamin B12-dependent methylmalonic aciduria. Hum. Mol. Genet. *11,* 3361-3369.

Fehling, C., Nilsson, B., and Jagerstad, M. (1979). Effect of vitamin B12 deficiency on energy-rich phosphates, glycolytic and citric acid cycle metabolites and associated amino acids in rat cerebral cortex. J. Neurochem. *32,* 1115-1117.

Ferrari, D., Stepczynska, A., Los, M., Wesselborg, S., and Schulze-Osthoff, K. (1998). Differential regulation and ATP requirement for caspase-8 and caspase-3 activation during CD95- and anticancer drug-induced apoptosis. J. Exp. Med. *188,* 979-984.

Froese, D.S. and Gravel, R.A. (2010). Genetic disorders of vitamin B(1)(2) metabolism: eight complementation groups--eight genes. Expert Rev. Mol. Med. *12,* e37.

Gomes, A.P., Ilter, D., Low, V., Drapela, S., Schild, T., Mullarky, E., Han, J., Elia, I., Broekaert, D., Rosenzweig, A., et al. (2022). Altered propionate metabolism contributes to tumour progression and aggressiveness. Nat.

Metab. *4,* 435-443.

Grassian, A.R., Parker, S.J., Davidson, S.M., Divakaruni, A.S., Green, C.R., Zhang, X., Slocum, K.L., Pu, M., Lin, F., Vickers, C., et al. (2014). IDH1 mutations alter citric acid cycle metabolism and increase dependence on oxidative mitochondrial metabolism. Cancer Res. *74,* 3317-3331.

Haiman, C.A., Han, Y., Feng, Y., Xia, L., Hsu, C., Sheng, X., Pooler, L.C., Patel, Y., Kolonel, L.N., Carter, E., et al. (2013). Genome-wide testing of putative functional exonic variants in relationship with breast and prostate cancer risk in a multiethnic population. PLoS Genet. *9,* e1003419.

Inigo, M., Deja, S., and Burgess, S.C. (2021). Ins and outs of the TCA cycle: the central role of anaplerosis. Annu. Rev. Nutr. *41,* 19-47.

Itatani, Y., Kawada, K., and Sakai, Y. (2019). Transforming growth factor-beta signaling pathway in colorectal cancer and its tumor microenvironment. Int. J. Mol. Sci. *20,* 5822.

Johnson, K., Kirkpatrick, H., Comer, A., Hoffmann, F.M., and Laughon, A. (1999). Interaction of Smad complexes with tripartite DNA-binding sites. J. Biol. Chem. *274,* 20709-20716.

Kishton, R.J. and Rathmell, J.C. (2015). Novel therapeutic targets of tumor metabolism. Cancer J. *21,* 62-69.

Lee, N. and Kim, D. (2016). Cancer metabolism: fueling more than just growth. Mol. Cells *39*, 847-854.

Lee, S.U., Kim, M.O., Kang, M.J., Oh, E.S., Ro, H., Lee, R.W., Song, Y.N., Jung, S., Lee, J.W., Lee, S.Y., et al. (2021). Transforming growth factor-b inhibits MUC5AC expression by SMAD3/HDAC2 complex formation and NF-kB deacetylation at K310 in NCI-H292 cells. Mol. Cells *44*, 38-49.

Lycan, T.W., Pardee, T.S., Petty, W.J., Bonomi, M., Alistar, A., Lamar, Z.S., Isom, S., Chan, M.D., Miller, A.A., and Ruiz, J. (2016). A phase II clinical trial of CPI-613 in patients with relapsed or refractory small cell lung carcinoma. PLoS One *11*, e0164244.

Massague, J. (1998). TGF-beta signal transduction. Annu. Rev. Biochem. *67*, 753-791.

Massague, J. and Wotton, D. (2000). Transcriptional control by the TGF-beta/Smad signaling system. EMBO J. *19*, 1745-1754.

McCarthy, A.J. and Chetty, R. (2018). Smad4/DPC4. J. Clin. Pathol. *71*, 661-664.

Miyaki, M. and Kuroki, T. (2003). Role of Smad4 (DPC4) inactivation in human cancer. Biochem. Biophys. Res. Commun. *306*, 799-804.

Papageorgis, P., Cheng, K., Ozturk, S., Gong, Y., Lambert, A.W., Abdolmaleky, H.M., Zhou, J.R., and Thiagalingam, S. (2011). Smad4 inactivation promotes malignancy and drug resistance of colon cancer. Cancer Res. *71*, 998-1008.

Pardee, T.S., Lee, K., Luddy, J., Maturo, C., Rodriguez, R., Isom, S., Miller, L.D., Stadelman, K.M., Levitan, D., Hurd, D., et al. (2014). A phase I study of the first-in-class antimitochondrial metabolism agent, CPI-613, in patients with advanced hematologic malignancies. Clin. Cancer Res. *20*, 5255-5264.

Pathania, D., Millard, M., and Neamati, N. (2009). Opportunities in discovery and delivery of anticancer drugs targeting mitochondria and cancer cell metabolism. Adv. Drug Deliv. Rev. *61*, 1250-1275.

Pavlova, N.N. and Thompson, C.B. (2016). The emerging hallmarks of cancer metabolism. Cell Metab. *23*, 27-47.

Phillips, D., Aponte, A.M., French, S.A., Chess, D.J., and Balaban, R.S. (2009). Succinyl-CoA synthetase is a phosphate target for the activation of mitochondrial metabolism. Biochemistry *48*, 7140-7149.

Plessl, T., Bürer, C., Lutz, S., Yue, W.W., Baumgartner, M.R., and Froese, D.S. (2017). Protein destabilization and loss of protein-protein interaction are fundamental mechanisms in cblA-type methylmalonic aciduria. Hum. Mutat. *38*, 988-1001.

Rajasekaran, N., Song, K., Lee, J.H., Wei, Y., Erkin, Ö.C., Lee, H., and Shin, Y.K. (2021). Nuclear respiratory factor-1, a novel SMAD4 binding protein, represses TGF-beta/SMAD4 signaling by functioning as a transcriptional cofactor. Int. J. Mol. Sci. *22*, 5595.

Rosenberg, L.E., Lilljeqvist, A.C., and Hsia, Y.E. (1968a). Methylmalonic aciduria. An inborn error leading to metabolic acidosis, long-chain ketonuria and intermittent hyperglycinemia. N. Engl. J. Med. *278*, 1319-1322.

Rosenberg, L.E., Lilljeqvist, A., and Hsia, Y.E. (1968b). Methylmalonic aciduria: metabolic block localization and vitamin B 12 dependency. Science *162*, 805-807.

Rush, E.C., Katre, P., and Yajnik, C.S. (2014). Vitamin B12: one carbon metabolism, fetal growth and programming for chronic disease. Eur. J. Clin. Nutr. *68*, 2-7.

Schutte, M. (1999). DPC4/SMAD4 gene alterations in human cancer, and their functional implications. Ann. Oncol. *10* Suppl *4*, 56-59.

Sorin, M., Watkins, D., Gilfix, B.M., and Rosenblatt, D.S. (2021). Methionine dependence in tumor cells: the potential role of cobalamin and MMACHC. Mol. Genet. Metab. *132*, 155-161.

Tsujimoto, Y. (1997). Apoptosis and necrosis: intracellular ATP level as a determinant for cell death modes. Cell Death Differ. *4*, 429-434.

Wan, R., Feng, J., and Tang, L. (2021). Consequences of mutations and abnormal expression of SMAD4 in tumors and T cells. Onco Targets Ther. *14*, 2531-2540.

Wilentz, R.E., Iacobuzio-Donahue, C.A., Argani, P., McCarthy, D.M., Parsons, J.L., Yeo, C.J., Kern, S.E., and Hruban, R.H. (2000). Loss of expression of Dpc4 in pancreatic intraepithelial neoplasia: evidence that DPC4 inactivation occurs late in neoplastic progression. Cancer Res. *60*, 2002-2006.

Williamson, J.R. and Cooper, R.H. (1980). Regulation of the citric acid cycle in mammalian systems. FEBS Lett. *117* Suppl, K73-K85.

Yan, P., Klingbiel, D., Saridaki, Z., Ceppa, P., Curto, M., McKee, T.A., Roth, A., Tejpar, S., Delorenzi, M., Bosman, F.T., et al. (2016). Reduced expression of SMAD4 is associated with poor survival in colon cancer. Clin. Cancer Res. *22*, 3037-3047.

Yen, K., Travins, J., Wang, F., David, M.D., Artin, E., Straley, K., Padyana, A., Gross, S., DeLaBarre, B., Tobin, E., et al. (2017). AG-221, a first-in-class therapy targeting acute myeloid leukemia harboring oncogenic IDH2 mutation. Cancer Discov. *7*, 478-493.

Yuneva, M.O., Fan, T.W., Allen, T.D., Higashi, R.M., Ferraris, D.V., Tsukamoto, T., Matés, J.M., Alonso, F.J., Wang, C., Seo, Y., et al. (2012). The metabolic profile of tumors depends on both the responsible genetic lesion and tissue type. Cell Metab. *15*, 157-170.

Zachar, Z., Marecek, J., Maturo, C., Gupta, S., Stuart, S.D., Howell, K., Schauble, A., Lem, J., Piramzadian, A., Karnik, S., et al. (2011). Non-redox-active lipoate derivatives disrupt cancer cell mitochondrial metabolism and are potent anticancer agents in-vivo. J. Mol. Med. (Berl.) *89*, 1137-1148.

Zamaraeva, M.V., Sabirov, R.Z., Maeno, E., Ando-Akatsuka, Y., Bessonova, S.V., and Okada, Y. (2005). Cells die with increased cytosolic ATP during apoptosis: a bioluminescence study with intracellular luciferase. Cell Death Differ. *12*, 1390-1397.

Zawel, L., Dai, J.L., Buckhaults, P., Zhou, S., Kinzler, K.W., Vogelstein, B., and Kern, S.E. (1998). Human Smad3 and Smad4 are sequence-specific transcription activators. Mol. Cell *1*, 611-617.

Zhang, J., Dobson, C.M., Wu, X., Lerner-Ellis, J., Rosenblatt, D.S., and Gravel, R.A. (2006). Impact of cblB mutations on the function of ATP:cob(I)alamin adenosyltransferase in disorders of vitamin B12 metabolism. Mol. Genet. Metab. *87*, 315-322.